Dynamic stall on an airfoil undergoing VAWT blade angle of attack variations

Dynamic stall on an airfoil undergoing VAWT blade angle of attack variations

Sabrina Henne, Sébastien Le Fouest, Karen Mulleners

Institute of mechanical engineering, École polytechnique fédérale de Lausanne, 1015 Lausanne, Switzerland

E-mail: karen.mulleners@epfl.ch

Abstract. Vertical axis wind turbines have several attractive features in the context of energy production in urban areas, but the inherent aerodynamic complexity of the flow around them has challenged their development on a larger scale. They generally operate at low tip speed ratios, where dynamic stall occurs on the blades. The vortex shedding associated with dynamic stall causes highly transient and heavy stress cycles that reduce the aerodynamic performance and increase the risk of fatigue and failure. The flow around an airfoil undergoing VAWT blade angle of attack variations was investigated using particle image velocimetry and force measurements. The formation of vortices and the lift force were studied for different tip speed ratios. A special focus was put on the effect of the asymmetry of the motion. The role of dynamic stall vortices on aerodynamic coefficients was evidenced by comparing experimental data to analytical predictions obtained from Theodorsen's model. For the lowest equivalent tip speed ratio clockwise and counter clockwise rotating dynamic stall vortices formed on the airfoil with increasing and decreasing angle of attack. The asymmetry in motion lead to an asymmetry in size of the clockwise and counter-clockwise vortices. As the asymmetry in motion has a strong effect on the flow behaviour, the local pitch rate was proposed as a governing parameter. The increase of extrema with increasing pitch rate varies for increasing and decreasing angle of attack, indicating an additional influence of the history of the flow development.

1. Introduction

Due to their aerodynamic complexity, vertical axis wind turbines (VAWT) are less well understood than conventional horizontal axis wind turbines (HAWTs). VAWT have several attractive features in the context of energy production in urban areas. They produce energy independently of the wind direction. Compared to their horizontal counterparts, they have fewer moving parts, generate less noise, and are able to operate at lower wind speeds. Their scalability is also an attractive trait for urban installation, as energy production tends to decentralise from large industrial plants to local generation and consumption. VAWT are more cost efficient at small scale than HAWTs [12, 4] and could be implemented on top of buildings or in street canyons [7].

The inherent aerodynamic complexity of the flow around VAWT has challenged their development for large scale power production. The blades of a VAWT rotate around an axis perpendicular to the free stream and the effective inflow velocity and angle of attack at the

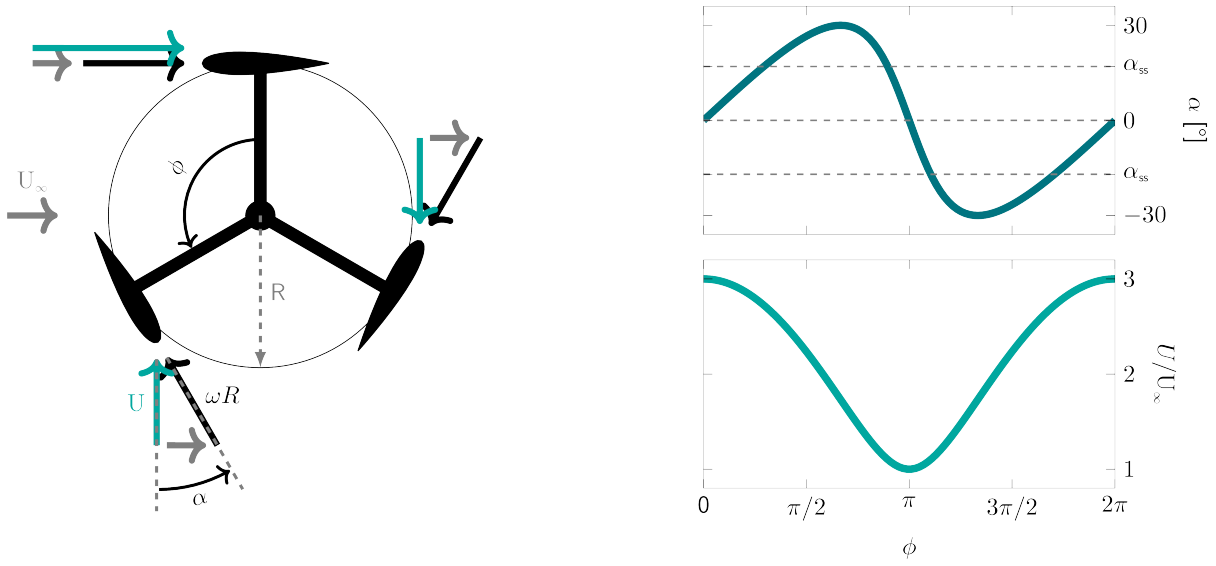

Figure 1. Schematic representation of the angle of attack and Reynolds number variations during a single rotation cycle for a VAWT at $\lambda = 2$.

blade level varies within one rotational cycle. The evolution of the effective angle of attack and the peak-to-peak amplitudes depend strongly on the ratio between the blade velocity and free stream velocity, known as tip-speed ratio. If we ignore the influence the turbine has on itself, we can represent the evolution of the effective angle of attack as

$$\alpha = \tan^{-1}\left(\frac{\sin(\phi)}{\lambda + \cos(\phi)}\right) \tag{1}$$

with λ the tip speed ratio and ϕ the angular position of the blade in the wind turbine [8]. An overview of the variations for a tip-speed ratio of $\lambda = 2$ is presented in figure 1. For a turbine operating at low tip-speed ratio, the blade exceeds its static stall angle α_{ss}, leading to dynamic stall [2]. This phenomenon is characterised by the formation, growth, and shedding of large scale dynamic stall vortices [10]. Vortex shedding causes highly transient and heavy stress cycles that reduce the aerodynamic performance and jeopardise the turbine's structural integrity increasing the risk of fatigue and failure [11]. To increase the efficiency of VAWT, it is desirable to improve our understanding and our ability to predict the development of dynamic stall.

Most investigations of dynamic stall focus on sinusoidally pitching airfoils, analysing the development of dynamic stall vortices during motions with different mean angles and amplitudes [3, 9]. Dunne and McKeon [5] consider a combined sinusoidally pitching and surging motion on a two-dimensional airfoil. This is an important step towards studying the combined influence of the inflow velocity and angle of attack variations experienced by the blades in a vertical axis wind turbine. The pitching kinematics considered in this study are still sinusoidal which leads to a symmetric motion and pitch rate evolution. A NACA0015 airfoil pitching with the angle of attack variation described in figure 1 was investigated by Angell et al. [1]. The data was collected as part of the Glasgow database for different wing profiles. Scheurich and Brown [14] use this data to validate their model for the normal and tangential force coefficients for VAWT blades. For moderate and low tip speed ratios (λ =2.7 and 3.4), a dynamic stall model needs to be considered to accurately model the experimental data. For the high tip speed ratio investigated (λ =4.85), no dynamic stall model is required.

The objective of our study is to characterise the influence of the asymmetric changes in angle of attack on the load cycles and on the development of dynamic stall. We experimentally investigate the flow and force response on an airfoil undergoing a pitching motion mirroring the angle of attack variation of a VAWT blade at a constant inflow velocity. The investigation offers insight on the importance of the asymmetry in the angle of attack variation. We also compute theoretical load fluctuations using Theodorsen's unsteady aerodynamic model [15]. This model is based on potential flow theory that assumes inviscid and fully attached flow. By comparing results we identify the influence of flow detachment and viscous effects on aerodynamic loads. VAWT blades follow a curved path. Coriolis effects act on the boundary layer of a rotating flow environment when observed from a fixed frame of reference. In this investigation we remove that additional complexity by performing the pitching motion in a translating frame of reference.

2. Methodology

Experiments were conducted in the SHARX recirculating water channel at EPFL. The channel has a $0.6\,\mathrm{m} \times 0.6\,\mathrm{m} \times 3\,\mathrm{m}$ test section and can reach a maximum free stream velocity of $U_\infty = 1\,\mathrm{m\,s^{-1}}$. The entire test section is constructed of plexiglass walls bounded by a metallic frame, providing uninterrupted optical access for optical velocity field measurements.

A NACA0018 airfoil with a chord length of $c = 0.15\,\mathrm{m}$ and span $s = 0.6\,\mathrm{m}$, yielding an aspect ratio of $AR = {}^{s}/_{c} = 4$, was suspended vertically in the water channel. The airfoil was 3D printed using PLA and covered with epoxy to ensure its persistence in water. A splitter plate was installed to reduce surface effects (figure 2). A 6-component ATI load cell was used to measure the forces at a sampling frequency of $f_s = 1\,\mathrm{kHz}$, with a sensing range of 125 N and a resolution of 0.02 N.

A high speed particle image velocimetry (PIV) system was set up to measure the flow field. A Photron Fastcam SA-X2, with a sensor size of $1024\,\mathrm{px} \times 1024\,\mathrm{px}$ and a 45° mirror were installed below the channel to capture the flow around the blade. A dual oscillator diode pumped ND:YLF laser ($\lambda = 527\,\mathrm{nm}$) with a maximum pulse energy of 30 mJ and a beam splitter were used to create two laser sheets from opposite sides of the channel. The light sheets were oriented horizontally at mid-span of the blades. For each measurement series 10 900 images were recorded at a frequency of 500 Hz, yielding a total measurement time of 21.8 s. The images were processed following standard procedures using a multigrid algorithm with image deformation [13]. The final window size was $48\,\mathrm{px} \times 48\,\mathrm{px}$ with an overlap of 66.6 %. This yields a grid spacing or physical resolution of $4.3\,\mathrm{mm} = 0.029c$.

The airfoil was actuated to undergo a pitching motion around its quarter chord. Similarity is maintained with a hypothetical single-bladed VAWT characterised by a chord-to-diameter ratio of $\frac{c}{D} = 0.15$. This yields a hypothetical radius of 0.375 m based on the blade's chord length. Note that the hypothetical solidity is equal to the chord-to-diameter ratio, as the hypothetical VAWT has a single blade. Experiments were performed at a fixed chord-based Reynolds number $Re = {}^{cU_\infty}/_{\nu} = 50\,000$. Four different tip speed ratios $\lambda \in \{1.5, 2, 2.5, 3\}$ were tested, screening the operation range of VAWT where dynamic stall is most common. From the tip speed ratio and calculated radius, we deduce the hypothetical VAWT rotational frequency and the temporal evolution of the pitch angle α using figure 1.

We investigate attached flow effects by comparing experimental results to loads computed using Theodorsen's model [15]. This model provides the unsteady lift coefficient for a flat plate undergoing harmonic pitching motions. We adapt the model to the asymetric VAWT angle variation by expressing the pitching motion as the sum of harmonic functions with increasing

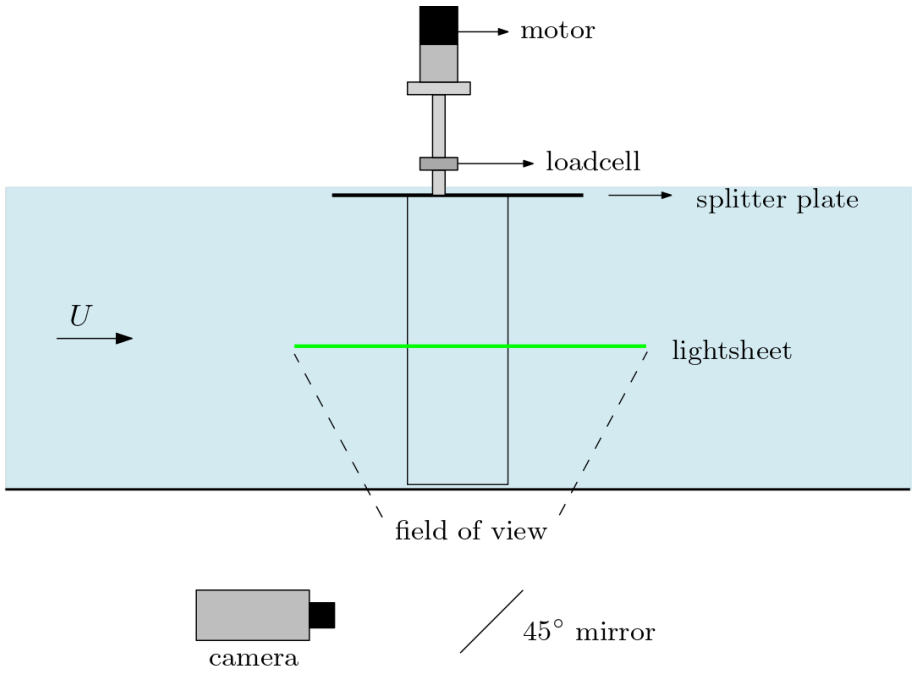

Figure 2. Experimental pitching airfoil set-up in the waterchannel with PIV equipment.

frequencies using a third order Fourier series fit. Theodorsen's solution is then:

$$C_L = \frac{\pi c\dot{\alpha}(t)}{2U_\infty} - 2\pi C(k)\left(\alpha(t) + \frac{c\dot{\alpha}(t)}{2U_\infty}\right) \tag{2}$$

where the reduced frequency is defined as $k = \frac{\pi\omega c}{U_\infty}$ and C is Theodorsen's complex transfer function. The first term is referred to as the pitching term and the second term is the circulatory term.

3. Results

The phase averaged force response, the angle of attack, and the dimensionless pitch rate for $\lambda = 1.5$ are presented in figure 3. The asymmetry of the motion increases with a decrease in tip speed ratio. We focus first on the lowest tested tip speed ratio to highlight the influence of the pitch rate asymmetry.

The angle of attack varies between $\alpha = -41.8°$ and $\alpha = 41.8°$. During the initial increase of the angle of attack, the dimensionless pitch rate $\dot{\alpha}c/(2U_\infty)$ is approximately constant until the maximum angle of attack is reached at $t/T = 0.37$. Thereafter, the dimensionless pitch rate decreases rapidly and reaches a minimum value of -0.61 at $t/T = 0.5$. At the start of the second half of the cycle, the pitch rate increases rapidly until the minimum angle of attack is reached at $t/T = 0.63$. In the last quarter of the cycle, the pitch rate reaches the same approximately constant value as in the beginning of the cycle.

The phase averaged lift response to this angle of attack evolution is included in figure 3. In the beginning of the cycle, the lift increases linearly with increasing angle of attack from 0° and reaches a maximum value of $C_{l,max} = 2.8$ at $\alpha = 37.6°$, which is $0.08T$ before the maximum angle of attack is reached. During the increase in angle of attack a clockwise rotating dynamic stall vortex is formed on the top side of the airfoil (figure 4a-b). It grows into a round shape and separates when the maximum angle of attack is reached. This is indicated by an accumulation

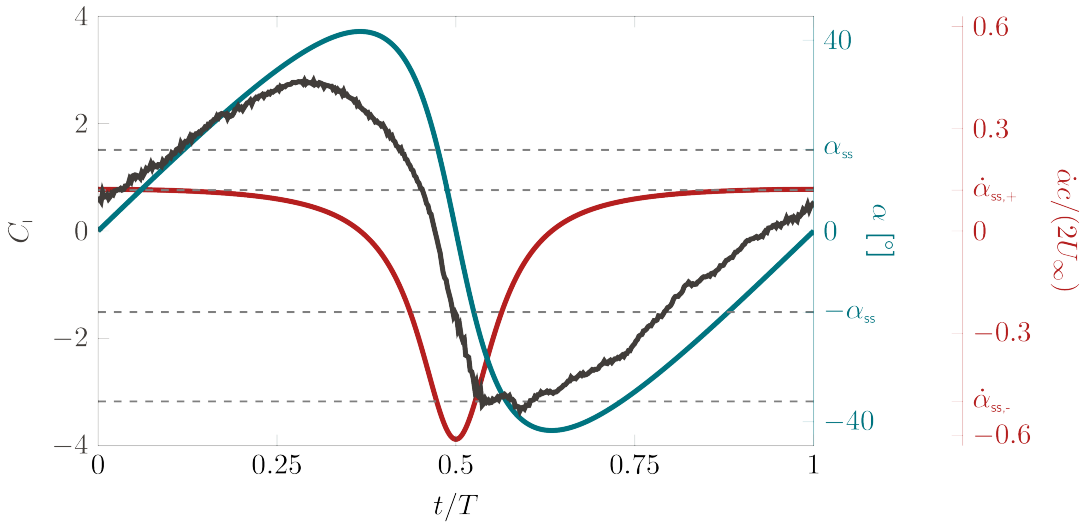

Figure 3. Phase averaged lift coefficient C_l, angle of attack α and dimensionless pitch rate $\dot{\alpha}$ over dimensionless time t/T for $\lambda = 1.5$

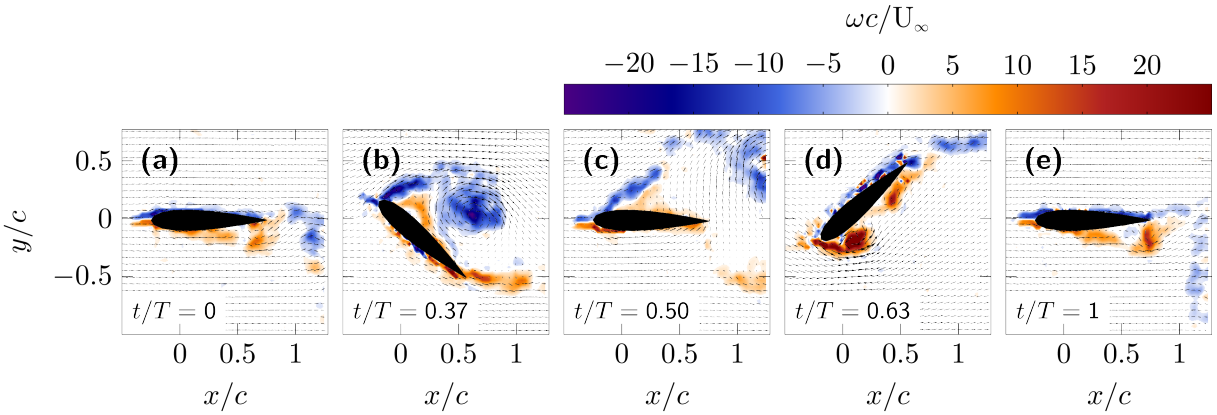

Figure 4. Snapshots of the velocity and vorticity field at selected time instants during a single pitching cycle for a tip speed ratio of $\lambda = 1.5$

of secondary positive vorticity between the coherent vortex and the airfoil's surface (figure 4b). After the maximum angle of attack is reached, the vortex is convected away from the airfoil. When the airfoil's angle of attack is decreased to negative values, the vortex has completely left the field of view (figure 4c). When the angle decreases below zero, a counter-clockwise rotating dynamic stall vortex is formed on the bottom side of the airfoil (figure 4d). The lift decreases rapidly with decreasing angle of attack and reaches a minimum value of $C_{l,min} = -3.5$ at $\alpha = 39.2°$, which is $0.04T$ before the minimum angle of attack is reached. When the airfoil reaches its minimum angle of attack, the vortex is still in an early stage of its growth and is not ready to shed. When the angle of attack increases again in the end of the cycle, the lift also increases again. The small counter-clockwise vortex is convected across the airfoil surface and shed into the wake (figure 4e).

The comparison of the experimental and analytical unsteady lift coefficient is shown in figure 5. The analytical model agrees very well with the experimental data for the two higher tip-speed

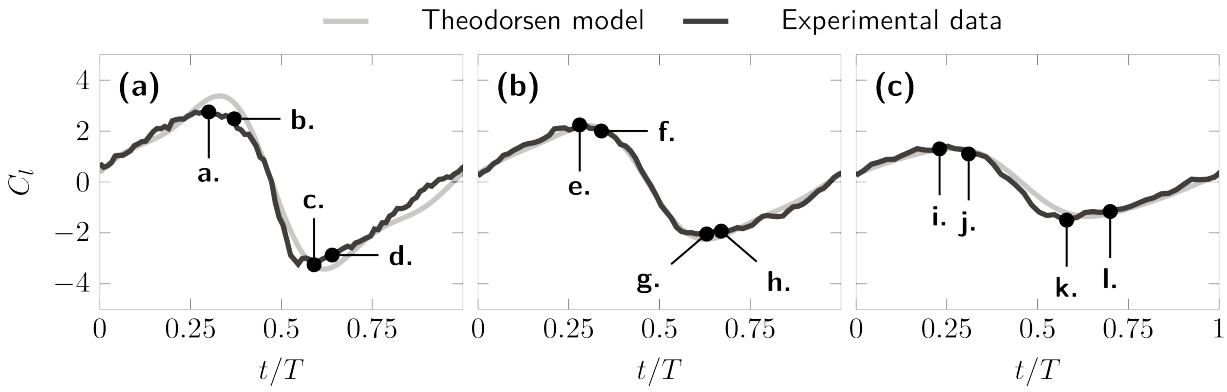

Figure 5. Unsteady lift coefficient C_L comparison for $\lambda = 1.5$ **(a)**, $\lambda = 2$ **(b)** and $\lambda = 3$ **(c)**

ratios $\lambda = 2$ and $\lambda = 3$, but differences are notable for $\lambda = 1.5$. The magnitudes of $|C_{l,min}|$ and $|C_{l,max}|$ are lower for the experimental data than for the analytical prediction for $\lambda = 1.5$. The experimental lift coefficient reaches a maxima slightly earlier that the results from Theodorsen's model. Both these differences are attributed to the formation of a dynamic stall vortex evidenced in the vorticity plots from figure 6a-d. Flow separation occurs after the blade exceeds the static stall angle, which happens twice per period. Between the time the blade exceeds its stall angle and the time when the blade reaches maximum lift, circulatory energy in the boundary layer is progressively stored in leading-edge vortices shown in figure 6a,d. This process limits the increase in lift coefficient magnitude, both for increasing and decreasing angles of attack. When the blade reaches its maximum angle of attack on the upstroke, the dynamic stall vortex is about to separate (figure 6b). The blade enters a deep stall regime, resulting in a lift deficit compared to analytical predictions. A similar process takes place during the downstroke. The second leading edge vortex does not have time to reach its full size before the blade reaches its maximum angle of attack (figure 6d). The blade enters a light stall regime and the difference with analytical results is smaller than for the upstroke. The inviscid flow assumption in Theodorsen's model impedes flow separation, so the lift coefficient increase to a higher value until α_{max} is reached, delaying the time where $|C_{l,min}|$ and $|C_{l,max}|$ occur compared to the experimental data. For the higher tip-speed ratio $\lambda = 2$ and $\lambda = 3$, no evidenced of the blade entering deep stall is observed (figure 6).

The analysis of the flow field shows a significant difference in the formation of dynamic stall vortices during the increase and decrease in angle of attack (figure 6). The clockwise and counter-clockwise vortices for both $\lambda = 1.5$ and $\lambda = 2$ are in different states of development when the maximum and minimum lift coefficients are reached. For both cases, the counter-clockwise vortices start to develop at higher angles of attack than the clockwise vortices. For $\lambda = 1.5$, a coherent clockwise rotating vortex can be identified when the lift maximum is reached. When the lift minimum is reached the shear layer has only started to roll up into a counter-clockwise rotating vortex (figure 6a vs. c). For $\lambda = 2$, when the lift coefficient maximum is reached, the clockwise rotating vortex only just began to form and keeps growing with increasing angle of attack (figure 6e-f). The counter-clockwise rotating vortex only becomes identifiable after the minimum lift coefficient is reached (figure 6e-f). For $\lambda = 3$, no coherent dynamic stall vortices can be identified (figure 6i-l). The accumulation of vorticity in the dynamic stall vortices is the main reason for the increase in lift in comparison to static stall lift values. As the vortices in these cases are different in size and position along the airfoil their influence on the lift will differ.

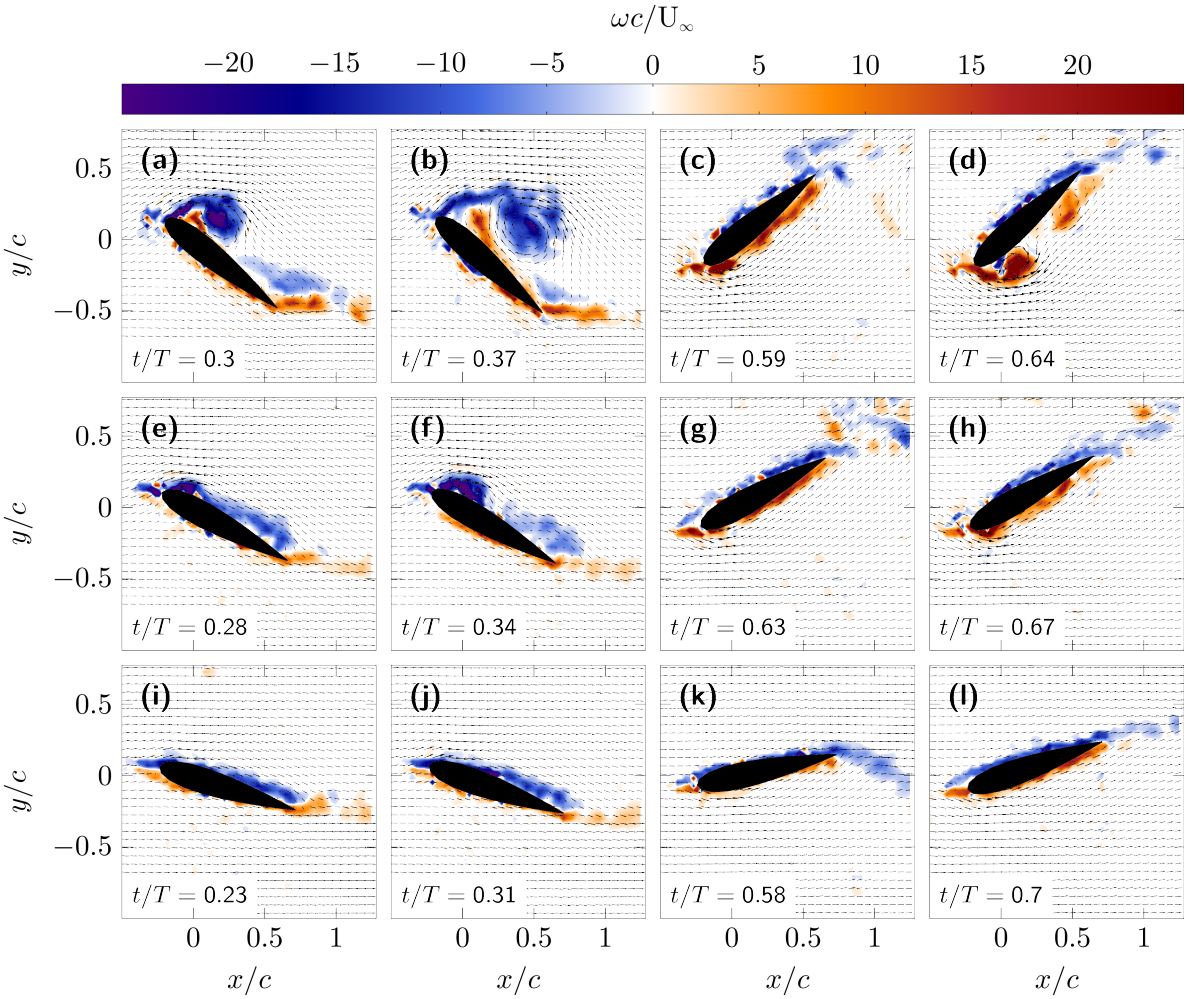

Figure 6. Snapshots of the velocity and vorticity fields at selected time instants during a single pitching cycle for $\lambda = 1.5$,$\lambda = 2$ and $\lambda = 3$

The magnitudes of the maximum and minimum lift coefficients are compared in figure 7a,b for the different pitching motions. The absolute values of the maximum and minimum in lift coefficient decrease with increasing tip speed ratio (figure 7a). For the two limiting cases $\lambda = 1.5$ and $\lambda = 3$, the magnitude of the minimum C_l is larger than the magnitude of the maximum C_l. For $\lambda = 2$, the magnitude of the maximum C_l is higher and for $\lambda = 2.5$ both reach approximately the same value. The influence of the stall vortices is higher for the increasing angle of attack and as the angle of attack is symmetric around zero, $\alpha_{max} = -\alpha_{min}$, the difference between $|C_{l,min}|$ and $|C_{l,max}|$ is due to the different evolution of the pitch rate leading up to the extrema. The difference in pitch rate between increasing and decreasing angle of attack is characterised by the local pitch rate of the airfoil when it passes the static stall angle $\dot{\alpha}_{ss,+}$ and $\dot{\alpha}_{ss,-}$.

The ratio $\Pi_{\alpha_{ss}} = |\dot{\alpha}_{ss,-}/\dot{\alpha}_{ss,+}|$ is defined to highlight the asymmetry in the pitch rate evolution. The $\Pi_{\alpha_{ss}}$-values for the different tip speed ratios $\lambda \in \{1.5, 2, 2.5, 3\}$ are $\{4.3, 2.5, 1.7, 1.4\}$. For the highest tip speed ratio, the static stall angle is crossed 1.4 times faster when the angle of attack decreases than when it increases. For the lowest tip speed ratio, the crossing happens 4.3 times faster when the angle of attack decreases. The time the airfoil needs to reach its maximum and minimum angle of attack differs. When regarding the magnitude of C_l with respect to the

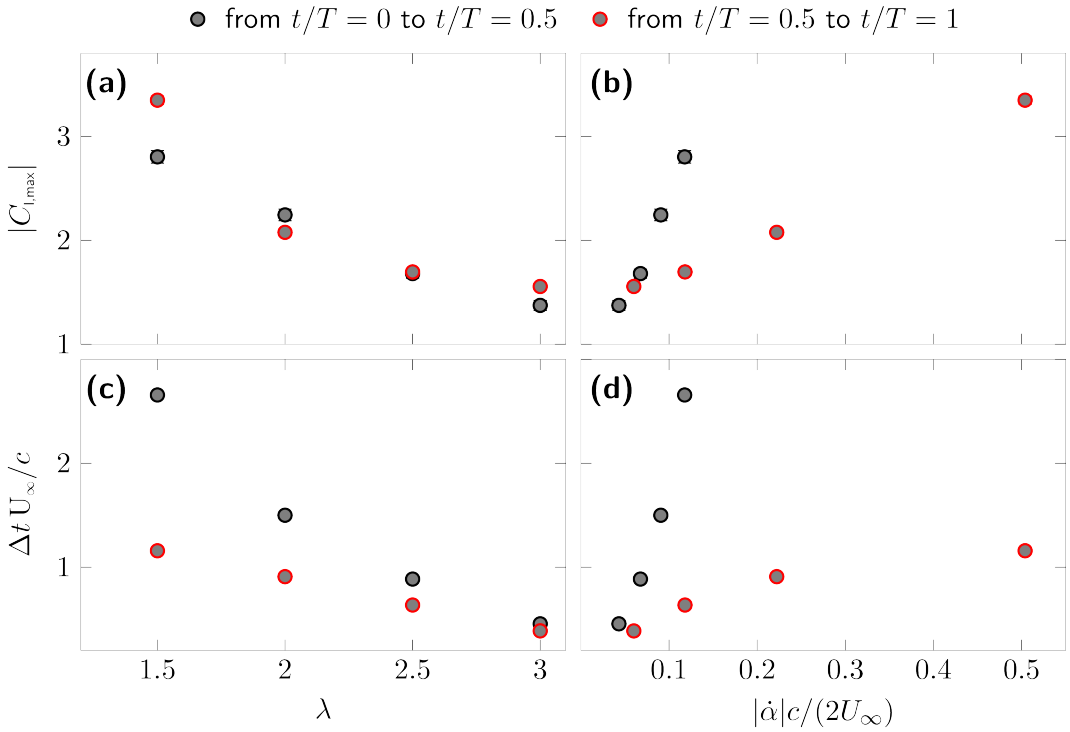

Figure 7. Magnitude of the maximum and minimum lift coefficient over tip speed ratio **(a)** and dimensionless pitch rate **(b)** and convective time difference between static stall angle and minimum/maximum angle of attack over tip speed ratio **(c)** and dimensionless pitch rate **(d)**.

local pitch rate, the highest lift coefficient value is reached for the highest pitch rate. The increase of the extrema with pitch rate varies for increasing and decreasing angle of attack. This is a results out of a combination of the differences in absolute maximum angle of attack, size and position of dynamic stall vortices and pitch rate effects. Higher local pitch rates yield higher extreme values but there is an additional influence of the history of the flow development that is not captured by the local pitch rate at the crossing of the static stall angle.

To further investigate the influence of the pitch rate, the convective time differences between the time when the static stall angle is crossed $t_{c,ss+/-}$ and the time at which the maximum angles $t_{c,max\pm}$ are reached are compared in figure 7c,d. These time differences give an idea of how much time the dynamic stall vortices have to develop before a change in pitch direction occurs and are a measure for the vortex age at pitch reversal. The convective time difference decreases with increasing tip speed ratio (figure 7c). The time between the crossing of the negative static stall angle and the minimum angle of attack is always smaller than that between the positive stall angle and the maximum angle of attack. For a tip speed ratio of $\lambda = 1.5$, the time difference between $\alpha_{ss,+}$ and α_{max} is $\Delta t_{c,ss+} = 2.74$. The time difference between $\alpha_{ss,-}$ and α_{min} is $\Delta t_{c,ss-} = 1.2$. The clockwise rotating vortex that grows with increasing angle of attack has more than double the time of the counter-clockwise rotating vortex to develop before the maximum angle is reached (figure 6a vs c). This explains why the clockwise rotating vortex is at the stage of separation whereas the counter-clockwise vortex is just starting to develop when the maximum respective minimum angle of attack is reached. As a consequence, the absolute value of the lift extrema is lower for positive angles of attack that for the negative angles of attack in the second part of the cycle.

Previous investigations on an airfoil undergoing a linear ramp-up motion by Henne et al. [6] have revealed that the dynamic stall vortex requires a minimum convective time to reach it maximum size and separate. This minimum convective time decreases with increasing pitch rate and becomes independent of the pitch rate for dimensionless pitch rates above 0.05 and reaches a value of approximately 5. The representative dimensionless pitch rates in the cases presented here are close to and above 0.05, with the lowest dimensionless pitch rate $|\dot{\alpha}_{ss,\pm}| = 0.04$ for $\lambda = 3$ and the highest 0.5 for $\lambda = 1.5$. For all cases the available convective time for the vortex to develop is less than 5 (figure 7d). The vortices do not have enough time to grow to their full potential and to shed naturally. Instead, the vortices are forced to separates shortly after the maximum or minimum angle of attack is reached and the direction of the angle of attack evolution has reversed. This behaviour is characteristic of light dynamic stall [9] and the lift evolution during light stall is still relatively well described by simple models such as Theodorsen's theory.

4. Conclusions

Particle image velocimetry and force measurements have been conducted to investigate the influence of an asymmetric angle of attack variation on the development of dynamic stall. The asymmetric angle of attack kinematics tested here represents the evolution in effective angle of attack that vertical axis wind turbine blades undergo during rotation. By subjecting a non-rotating blade to these kinematics, we focus purely on the influence of the asymmetry of the pitching motion on the unsteady lift response and flow development around the blade. Experiments were conducted for four different conditions corresponding to equivalent tip speed ratios ranging from $\lambda = 1.5$ to $\lambda = 3$. The degree of asymmetry of the motion increases with decreasing tip speed ratio. The role of dynamic stall vortices on aerodynamic coefficients was evidenced by comparing experimental data to analytical predictions obtained from Theodorsen's model. For the lowest two tip speed ratios, clockwise and counter-clockwise rotating dynamic stall vortices were observed, limiting the maximum lift coefficient reached compared to the analytical results. For the two higher tip speed ratios, no dynamic stall vortices were observed and the lift response is well predicted by Theodorsen's model. The asymmetry in the motion leads to an asymmetry in the clockwise and counter-clockwise rotating dynamic stall vortices that form on the blade with increasing and decreasing angle of attack. The local pitch rate during the negative angle of attack motion is higher than during the positive angle of attack motion, yielding smaller counter-clockwise rotating dynamic stall vortices than their clockwise rotating counterparts. The influence of the counter-clockwise rotating vortices on the lift is therefore smaller and the lift evolution follows the predictions by the Theodorsen model and reaches higher absolute values for the pitching down part of the cycle.

Acknowledgments

This work is supported by the Swiss national science foundation (SNSF) Assistant Professor energy grant number PYAPP2_173652.

References

[1] R. K. Angell, P. J. Musgrove, and R. A. M. Galbraith. Collected data for tests on a naca 0015—volume iii: Pressure data relevant to the study of large scale vertical axis wind turbines. *University of Glasgow, Glasgow, Scotland, Technical Report*, (8802), 1988.

[2] Abel-John Buchner, Julio Soria, Damon Honnery, and Alexander J. Smits. Dynamic stall in vertical axis wind turbines: scaling and topological considerations. *Journal of Fluid Mechanics*, 841:746–766, 2018.

[3] Lawrence W. Carr. Progress in analysis and prediction of dynamic stall. *Journal of aircraft*, 25(1):6–17, 1988.

[4] Tanate Chaichana and Sumpun Chaitep. Wind power potential and characteristic analysis of Chiang Mai, Thailand. *Journal of Mechanical Science and Technology*, 24(7):1475–1479, 2010.

[5] Reeve Dunne and Beverley J. McKeon. Dynamic stall on a pitching and surging airfoil. *Experiments in Fluids*, 56(8):157, 2015.

[6] Sabrina Henne, Agastya Parikh, Julien Deparday, and Karen Mulleners. Dynamic stall vortex shedding and associated load fluctuations. In *19th International Symposium of the Applications of Laser and Imaging Techniques to Fluid Mechanics*, 2018.

[7] Rakesh Kumar, Kaamran Raahemifar, and Alan S. Fung. A critical review of vertical axis wind turbines for urban applications. *Renewable and Sustainable Energy Reviews*, 89: 281–291, 2018.

[8] A. Laneville and P. Vittecoq. Dynamic stall: The case of the vertical axis wind turbine. *Journal of Solar Energy Engineering*, 108(2):140–145, 1986.

[9] Karen Mulleners and Markus Raffel. The onset of dynamic stall revisited. *Experiments in Fluids*, 52(3):779–793, 2011.

[10] Karen Mulleners and Markus Raffel. Dynamic stall development. *Experiments in Fluids*, 54(2):1469, 2013.

[11] Pablo Ouro, Thorsten Stoesser, and Luis Ramírez. Effect of blade cambering on dynamic stall in view of designing vertical axis turbines. *Journal of Fluids Engineering*, 140(6): 061104, 2018.

[12] Sayyad Basim Qamar and Isam Janajreh. A comprehensive analysis of solidity for cambered darrieus VAWTs. *International Journal of Hydrogen Energy*, 42(30):19420–19431, 2017.

[13] Markus Raffel, Christian E. Willert, Steve T. Wereley, and Jürgen Kompenhans. *Particle image velocimetry*. Springer Verlag, 2007.

[14] Frank Scheurich and Richard E. Brown. Effect of dynamic stall on the aerodynamics of vertical-axis wind turbines. *AIAA Journal*, 49(11):2511–2521, 2011.

[15] Theodore Theodorsen. General theory of aerodynamic instability and the mechanism of flutter. Technical report, National Advisory Committee for Aeronautics, 1935.